Published in final edited form as:
Dev Dyn. 2011 April ; 240(4): 839–849. doi:10.1002/dvdy.22577.

A novel hypomorphic *Looptail* allele at the planar cell polarity *Vangl2* gene

Marie-Claude Guyot[1], **Ciprian M. Bosoi**[1], **Fares Kharfallah**[1], **Annie Reynolds**[1], **Pierre Drapeau**[2], **Monica Justice**[3], **Philippe Gros**[4], and **Zoha Kibar**[1,*]

[1]Department of Obstetrics and Gynecology, CHU Sainte Justine Research Center and University of Montreal

[2]Department of Pathology and Cell Biology, University of Montreal, Montreal, Canada

[3]Department of Molecular and Human Genetics, Baylor College of Medicine, Houston, Texas, USA

[4]Department of Biochemistry, McGill University, Montreal, QC, Canada

Abstract

Vangl2 forms part of the planar cell polarity signalling pathway and is the gene defective in the *Looptail* (*Lp*) mouse mutant. Two previously described alleles, *Lp* and Lp^{m1Jus}, segregate in a semi-dominant fashion, with heterozygotes displaying the looped-tail appearance, while homozygotes show the neural tube defect called craniorachischisis. Here, we report a novel experimentally-induced allele, Lp^{m2Jus}, that carries a missense mutation, R259L, in *Vangl2*. This mutation was specific to the *Lp* phenotype and absent from both parental strains and 28 other inbred strains. Notably, this mutation segregates in a recessive manner with all heterozygotes appearing normal and 47% of homozygotes showing a looped-tail. Homozygous Lp^{m2Jus} embryos showed spina bifida in 12%. Lp^{m2Jus} genetically interacts with *Lp* with 77% of compound heterozygotes displaying craniorachischisis. $Vangl2^{R259L}$ behaved like the wild-type allele in overexpression and morpholino knockdown/rescue assays in zebrafish embryos. These data suggest that Lp^{m2Jus} represents a new hypomorphic allele of *Lp*.

Keywords

Looptail; *Vangl2*; planar cell polarity; neural tube defects; ENU mutagenesis

INTRODUCTION

Planar cell polarity (PCP) is the process by which cells become polarized in the plane of an epithelium. This process has been well studied in the adult epithelial tissues of *Drosophila* where it can be observed in the distal orientation of wing hairs, the posterior orientation of the abdominal bristles and the complex organization of the ommatidia (eye units) in the adult eye. Genetic studies of a wide range of mutants affecting these highly organized structures in the fly have identified a group of so called “core” PCP genes which includes *stbm/vang, frizzled* (*fz*), *dishevelled* (*dvl*), *flamingo* (*fmi*) *prickle* (*pk*) and *diego* (*dg*) (Simons and Mlodzik, 2008; Vladar et al., 2009). In mammalian tissues, PCP is observed in the inner ear sensory organs or the fur on an animal’s back. In particular, the auditory

*Correspondence to Zoha Kibar, University of Montreal, Department of Obstetrics and Gynecology, CHU Sainte Justine Research Center, 3175 Cote-Ste-Catherine, Room A711, Montreal, QC H3T 1C5 Canada; Tel: (514) 345 4931 X 3984; Fax: (514) 345 4801; zoha.kibar@recherche-ste-justine.qc.ca.

sensory organ in the cochlea displays a precise planar organization of its sensory hair cells that is essential for its proper function. The cochlea has one row of inner hair cells and three rows of outer hair cells, which are interdigitated with non-sensory support cells. Each hair cell projects microvilli-derived stereocilia that are arranged in order of increasing height toward the edge of the apical cortex to form a “V”-shaped structure with a single primary cilium, known as the kinocilium, placed near the tallest stereocilia at the vertex of the “V”-shaped stereociliary bundle. The vertices of the hair bundles all point toward the periphery of the cochlea, thus manifesting planar polarity. This planar organization is disrupted in single and double PCP mutants (Wang et al., 2006; McNeill, 2010).

In vertebrates, PCP proteins are also involved in the morphogenetic process of convergent extension (CE) that is critical for proper gastrulation and formation of the neural tube (Wang and Nathans, 2007). During this complex process, cells elongate medio-laterally and produce oriented cytoplasmic protrusions that enable them to move directionally and to intercalate with other neighboring cells. This leads to convergence of the tissue towards the midline and its extension along the anteroposterior axis (Keller et al., 2008). Evidence for involvement of PCP signaling in CE in vertebrates has initially emerged from studies of a wide range of mutants and morpholino-oligonucleotide (MO) knockdowns of orthologs of fly PCP genes in zebrafish and frog models. Embryos with defective PCP signaling caused by gene knockdown or overexpression manifest a well described CE defect depicted by marked shortening of the anterior–posterior axis (Wallingford, 2005). In mammals, Looptail (Lp) was the first mouse mutant to implicate a role of PCP and CE in neural tube defects (Kibar et al., 2001b; Murdoch et al., 2001a). A direct study of CE in vitally labeled pre-neurulation stage *Lp/Lp* embryos demonstrated a defective midline extension in the axial mesoderm and neural plate of these mutant embryos (Ybot-Gonzalez et al., 2007). Mutations in other vertebrate PCP genes cause various forms of NTDs in mouse (Wang and Nathans, 2007). Rare and novel missense mutations in *VANGL2* or its homologue *VANGL1* are associated with NTDs in humans (Kibar et al., 2007, 2009, 2010; Lei et al., 2010).

The *Lp* mouse represents a well-established model for the study of neural tube defects in humans (NTDs), the most common and severe malformations of the central nervous system in humans (1-2/1000 livebirths) (Bassuk and Kibar, 2009). *Lp* heterozygous mice are characterized by a kinked or looped-tail appearance while homozygous embryos die *in utero* suffering from a severe form of NTDs called craniorachischisis where the neural tube remains open throughout the hindbrain and spinal cord region (Strong and Hollander, 1949). *Lp* homozygous embryos also show failure of eyelid closure, outflow tract defects in the heart, severe inner ear polarity defects, and imperforate vagina in affected females (Henderson et al. 2001; Montcouquiol et al., 2003; VandenBerg and Sassoon, 2009). Two independent alleles have been described for the *Lp* mice: a naturally occurring *Lp* and a chemically induced Lp^{m1Jus} that both are transmitted in a semi-dominant fashion and produce identical phenotypes in heterozygotes (looped tail) and homozygous embryos (craniorachischisis) (Strong and Hollander, 1949; Kibar et al., 2001a). Positional cloning studies have identified *Vangl2* as the gene mutated in *Lp* mice (Kibar et al., 2001b; Murdoch et al., 2001a). *Vangl2* is strongly expressed in the neuroectoderm throughout neurulation and is altered in *Lp* where two disease-specific mutations, S464N and D255E, were identified in *Lp* and Lp^{m1Jus} respectively (Kibar et al., 2001b). *Vangl2* encodes a membrane protein whose predicted features include 4 transmembrane (TM) domains and a PDZ-domain binding motif at the carboxy terminus involved in protein-protein interaction (Torban et al., 2004).

Several studies were conducted to investigate the molecular mode of action of the two mutations, D255E and S464N, identified in *Vangl2* in Lp mice. Since these mutations map to different parts of the protein yet they produce identical phenotypes, it was hypothesized

that *Vangl2* acts a rate-limiting factor in a dosage sensitive pathway (Kibar et al., 2001b). In zebrafish embryos, both *Lp* mutations fail to rescue the CE defect caused by a MO-knockdown of the *tri* gene (tri, orthologue of *Vangl2*) and fail to produce a CE defect when over-expressed, strongly suggesting that they present loss-of-function mutations (Reynolds et al., 2010). Both mutations affect the interaction of Vangl1/2 with the Dishevelled PCP genes, which is critical for PCP signaling (Torban et al., 2004; Suriben et al., 2009). A recent study showed that Vangl2^{D255E} and Vangl2^{S464N} fail to sort into COPII vesicles and are trapped in the endoplasmic reticulum (Merte et al., 2010). A parallel study showed that the targeting of the Vangl2^{D255E} at the plasma membrane is greatly reduced where it is predominantly retained intracellularly in endoplasmic reticulum (ER) vesicles (Gravel et al., 2010). These studies highlight a critical role for D255 and S464 for normal folding and processing of Vangl proteins.

In this study, we report a new recessive missense mutation in *Vangl2*, R259L, that was generated in a large-scale phenotype-driven screen of mice mutagenized with N-ethyl-N-nitrosourea (ENU). Homozygous mice showed a looped tail appearance (47%), spina bifida (12%) but no craniorachischisis, and no significant PCP inner ear defects. Also, 78% of homozygous adult females exhibited imperforate vagina. All wild-type and heterozygous mice were apparently healthy. *Vangl2^{R259L}* genetically interacts with *Vangl2^{S464N}*, causing the severe craniorachischisis and PCP inner ear defect in compound heterozygous embryos. The *Vangl2^{R259L}* variant was able to rescue the *tri*-MO induced CE defect and produce a severe phenotype when overexpressed. These data strongly suggest that *Vangl2^{R259L}* represents a hypomorphic allele at the *Lp* termed *Lp^{m2Jus}*, where dosage is an important modulator of the severity of the PCP and CE-related phenotypes.

RESULTS

Molecular studies of *Lp^{m2Jus}*

The open reading frame and the exon-intron junctions of *Vangl2* were sequenced in *Lp^{m2Jus}* mouse with a looped tail phenotype and a single homozygous mutation, c.776 G>T, which changes arginine 259 to leucine (R259L), was identified. This mutation was absent from both parental strains and 28 other inbred strains, confirming its specificity to the *Lp* phenotype (and not a rare variant). The variant R259L resides in the predicted cytoplasmic domain of Vangl2 (Fig. 1A), just three amino acids away from the *Vangl2^{D255E}* mutation previously identified in *Lp^{m1Jus}*. R259 is invariant in all known orthologs except in zebrafish Vangl1 where it is replaced by histidine. Substitution of histidine preserves the basic nature of arginine, a physical property that is completely lost by the non conservative R259L substitution (Fig. 1B).

To determine whether R259L has any pathogenic effect on *Vangl2* gene expression, real-time RT-PCR was conducted to determine *Vangl2* mRNA levels in brain tissues of wild-type and homozygous mutant E16.5 embryos. The levels of *Vangl2* mRNA in mutant embryos were not significantly different from wild-type levels (Fig. 1C). To investigate whether the missense mutation R259L causes a decrease in Vangl2 protein levels, we performed western blot analysis on brain tissues from wild-type and homozygous mutant *Lp^{m2Jus}* E16.5 embryos, who are on a mixed B6 and 129 background. As reference and additional controls, we included wild-type, heterozygous *Lp*/+ and homozygous *Lp/Lp* mice, which are on a mixed A/J and B6 background. In brain, *Lp^{m2Jus}*/ *Lp^{m2Jus}* had 90% of Vangl2 protein as compared to their wild-type littermates (t-test, P=0.06) (Fig. 1D). However, protein levels were reduced by 32% in *Lp*/+ heterozygotes (t-test, P<0.001) and almost completely eliminated in *Lp/Lp* homozygous embryos (t-test, P<0.0001), as compared to their wild-type littermates (Fig.1D). A very faint band could be detected in *Lp/Lp* homozygous brain tissues upon longer exposure (data not shown).

We next examined Vangl2 protein expression pattern in the neural tube of E9.5 wild type and Lp^{m2Jus}/Lp^{m2Jus} embryos. Vangl2 was detected around the membrane of neuroepithelial cells, and no clear difference in expression pattern or levels was observed in the mutant embryos (Fig. 2).

Genotype-phenotype studies of the Lp^{m2Jus} allele

Lp^{m2Jus} N1F1 mutants were archived as frozen sperm and were consequently recovered at The Jackson Laboratory (http://jaxmice.jax.org/services/) by using the Assisted In Vitro Fertilization (AIVF) method. A total of 13 female and 15 male mice were generated following this procedure; all were heterozygotes for the R259L mutation and all had a normal appearance and breeding performance. These founder mice were used for expansion and maintenance of the Lp^{m2Jus} mutant line. In addition to these 28 founder mice, a total of 213 mice were generated over 4 generations and were examined for the presence of NTDs (Table 1). Crosses between parents that were heterozygotes at the mutant locus ($Lp^{m2Jus}/+$) generated a total of 164 litters including 36 wild-type, 85 heterozygotes and 43 homozygotes at the R259L mutation. The distribution of genotypes in these litters did not significantly differ from the expected Hardy-Weinberg ratio of 1:2:1 (χ^2 test, P=0.66). Matings between heterozygote and homozygote parents at the mutant locus generated 49 animals including 28 heterozygote and 21 homozygote mice. This genotype distribution was also not significantly different from the expected Hardy-Weinberg ratio of 1:1 (χ^2 test, P=0.39), suggesting that homozygosity for $Vangl2^{R259L}$ has no effect on viability or embryonic development. The Lp^{m2Jus} R259L mutation showed a recessive mode of inheritance where all wild-type and heterozygote mice were phenotypically normal and 47% (30/64) of homozygous adult mice had a looped or kinky tail appearance (Table 1). These results suggest incomplete penetrance of the R259L mutation on the mixed C57BL/6J; 129S6/SvEvTac genetic background.

In addition, 78% (21/27) of homozygous adult females showed imperforate vagina and 32% (12/37) of homozygote adult males appeared to be infertile (Table 1). All infertile Lp^{m2Jus} male were able to set copulatory plugs. A whole body necropsy analysis showed no histological differences between Lp^{m2Jus} homozygous infertile mice (n=2) and their wild-type littermates (n=2) (data not shown). Sperm assessment revealed no evidence for defective spermatogenesis and spermiogenesis since adequate and even superior sperm quality was observed in of Lp^{m2Jus} homozygous infertile mice as compared to wild-type littermates (data not shown).

The two previously described mutations in *Vangl2*, D225E and S464N, cause severe embryonic lethal craniorachischisis and failure of eyelid closure in homozygous embryos (Kibar et al., 2001a,b). Consequently, we examined Lp^{m2Jus}/Lp^{m2Jus} embryos for these two phenotypes. A total of 156 E12.5-E18.5 embryos were generated which included 37 wild-type, 69 heterozygous and 50 homozygous embryos for the R259L mutation. Interestingly, 12% (6/50) of the R259L homozygous embryos showed spina bifida characterized by an open neural tube in the lumbosacral region of the spinal cord (Table 1, Fig.3A). Histological sections across spinal regions of affected embryos revealed widely spaced neural folds characteristic of spina bifida (data not shown). In PCP mouse mutants, including *Lp*, a defective CE leads to a broad embryonic midline thus preventing the onset of neurulation through wide spacing of the neural folds (Ybot-Gonzalez et al., 2007). None of R259L homozygous embryos showed the more severe craniorachischisis NTD. In addition, all homozygous Lp^{m2Jus}/Lp^{m2Jus} embryos had normal eyelid closure (Fig. 3A). All wild-type and heterozygous embryos were apparently normal (Table 1).

Complementation studies with the Lp and Vangl1^{gt} alleles

Phenotype complementation studies were conducted between *Lp*^{m2Jus} and the previously described *Lp* Jackson allele caused by the *Vangl2* mutation S464N. Heterozygous *Lp*/+ mice were crossed to *Lp*^{m2Jus}/+ mice and embryos were recovered at various stages and examined macroscopically for the presence of NTDs and eyelid closure defects. A total of 13 compound heterozygous *Lp*^{m2Jus}/+; *Lp*/+ embryos were generated. Of these, 10 embryos exhibited the full-blown phenotype of craniorachischisis seen in *Lp/Lp* embryos and 2 embryos showed spina bifida, resulting in a penetrance of 92% (12/13) of the NTD phenotype in these compound heterozygotes for the S464N and R259L mutations at the *Vangl2* locus (Fig. 3B). Eyelid closure phenotype was examined in E18.5 embryos. Both compound heterozygotes with spina bifida had normal eye lid closure, while 60% (3/5) of compound heterozygotes with craniorachischisis exhibited unfused eyelids. These results demonstrate that *Lp*^{m2Jus} genetically interacts with the original *Lp* allele and contributes to the development of the severe NTD. These complementation studies together with the disease-specific nature of R259L strongly suggest that *Lp*^{m2Jus} is a new allele at the Lp locus.

Phenotype complementation studies were also conducted between *Lp*^{m2Jus} and the *Vangl1*^{gt} gene trap allele. *Vangl1*^{gt} heterozygotes and *Vangl1*$^{gt/gt}$ homozygotes were viable and fertile, as previously described. *Lp*^{m2Jus}/ *Lp*^{m2Jus} mice were mated to *Vangl1*$^{gt/gt}$ homozygotes and a total of 23 double heterozygous embryos were generated and examined macroscopically for the presence of NTDs and eyelid closure defects. All embryos were apparently normal with no looped tail or NTD or eyelid closure defect detected (Fig. 3C).

Analysis of the stereociliary bundle orientation in Lp^{m2Jus}

We next analyzed the effect of the R259L mutation on PCP regulation *in vivo* in the inner ear in *Lp*^{m2Jus} mutants and *Lp*^{m2Jus}/+; *Lp*/+ compound heterozygotes. We examined cochleae isolated from wild-type, *Lp*^{m2Jus} /+, *Lp*^{m2Jus}/ *Lp*^{m2Jus} and *Lp*^{m2Jus}/+; *Lp*/+ E18.5 embryos. Upon gross examination, the cochlear size of all mutant animals did not differ from those of the wild-type (data not shown). Examination of the inner (IHCs) and outer hair cells (OHCs) at the apical regions of the organ of Corti revealed no statistically significant difference between wild-type and each of the *Lp*^{m2Jus}/+ (data not shown) and *Lp*^{m2Jus}/ *Lp*^{m2Jus} cochlea (Fig. 4). In *Lp*^{m2Jus}+/-; *Lp*+/-compound heterozygotes, bundle orientation in OHC2 and OHC3 at the apical regions of the organ of Corti was severely affected (P=0.005) as compared to wild-type controls (Fig.4), confirming genetic interaction between *Lp* and *Lp*^{m2Jus}.

Examination of the inner ear of *Lp*^{m2Jus}/+; *Vangl1*^{gt}/+ double heterozygotes revealed no difference from the wild-type (data not shown), further demonstrating that both alleles fail to interact in these mutants.

Functional studies of VANGL2^{R259L} in the zebrafish model

We next validated the potential pathogenic effect of the R259L mutation on protein function *in vivo* by investigating its effect on convergent extension (CE) in zebrafish. Overexpression of *tri* impairs CE in zebrafish embryos and causes a reduction in axial length (Jessen et al., 2002; Park and Moon, 2002). We have shown previously that both Lp mutations D255E and S464N failed to induce a CE defect, as compared to wild-type, providing strong evidence that they act as loss-of-function alleles (Reynolds et al., 2010). We carried out an overexpression assay with wild-type *VANGL2, VANGL2*^{R259L}, and as additional references, *VANGL2*^{D255E} and *VANGL2*^{S464N}. When wild-type *VANGL2* was overexpressed, a severe reduction in axial length was observed as expected (P<0.001) (Fig. 5). Surprisingly, *VANGL2*^{R259L} behaved as the wild-type *VANGL2* and induced a severe

CE defect as well (P<0.001) (Fig. 5A,B). Injection of wild-type *Vangl2* or *VANGL2*^{R259L} at lower doses of 50 and 100 pg also caused a similar severe CE defect (P<0.01 and P<0.001 respectively) (Supplementary Fig.1). As expected, *VANGL2*^{D255E} and *VANGL2*^{S464N} failed to induce a CE defect and were statistically significant from *VANGL2* alone (P<0.001) (Fig. 5). Injection of 200 pg wild-type *VANGL2* alone produced a range of phenotypes that were clustered into three groups based on the phenotype severity (Fig. 5C). We examined the distributions of these three clusters among all 5 groups described above. The distribution of the clusters obtained with wild-type *VANGL2* or *VANGL2*^{R259L} was significantly different from uninjected wild-type fish (P<0.05) (Fig.5C). On the other hand, the distribution of the 3 clusters obtained from overexpression of either *VANGL2*^{D255E} or *VANGL2*^{S464N} was similar to uninjected fish and was significantly different than that obtained with wild-type *VANGL2* (P<0.05).

To substantiate the data obtained with the overexpression of *VANGL2*^{R259L}, a tri-*MO* knockdown/rescue assay was conducted (Fig. 6). When embryos were injected with *tri*-MO and raised until 2 days post fertilization, a severe (43%) decrease in length of the anterior-posterior axis in *tri*-MO fish was observed (P<0.001) (Fig. 6), consistent with previous findings (Jessen et al., 2002; Park and Moon, 2002). When co-injecting embryos with *tri*-MO and human *VANGL2* RNA, the average body length of *tri*-MO/*VANGL2* fish was significantly increased (P<0.05) (Fig. 6). Co-injection of *tri*-MO with *VANGL2*^{R259L} also was also able to rescue the CE defect suggesting that this variant is still functional (P<0.01) (Fig.6).

DISCUSSION

In this study, we identified and characterized a novel ENU-induced allele (*Lp*^{m2Jus}) at the *Vangl2* locus caused by the R259L missense mutation. This mutant represents a hypomorphic allele with a recessive mode of inheritance, as compared to the two other previously described Lp alleles (*Lp* and *Lp*^{m1Jus}) that segregated in a semi-dominant fashion (Kibar et al., 2001a,b). *Vangl2*^{R259L} caused a milder NTD defect in *Lp*^{m2Jus} mutants manifested by a looped or kinky tail in 47% of adult homozygotes and spina bifida in 12% of homozygous embryos as compared to the two previously described *Vangl2* mutations, *Vangl2*^{S464N} in *Lp* and *Vangl2*^{D255E} in *Lp*^{m1Jus}. In fact, two copies of the *Vangl2*^{R259L} mutation were needed to exert this phenotype that is usually caused by one copy of either of the *Vangl2*^{S464N} or *Vangl2*^{D255E} mutation. No craniorachischisis or eyelid closure defect was detected in *Vangl2*^{R259L} homozygotes. Examination of the inner ear also revealed no PCP defects in homozygous *Vangl2*^{R259L} embryos, similar to *Lp* heterozygous mice. This mild NTD phenotype and the absence of a PCP phenotype could be explained by a milder functional defect of the *Vangl2*^{R259L} where the dosage is less limiting than that of either the two other *Vangl2* mutations and/or that there may be different genetic modifiers in the different backgrounds of the 3 mutants.

The phenotype detected in the mutant argues against a dominant negative mode of action for the R259L mutation since heterozygotes do not have an NTD phenotype. Our zebrafish validation data favor the hypothesis of a weak hypomorphic allele at *Lp*^{m2Jus} where *Vangl2*^{R259L} behaves like the wild-type in overexpression (even at low doses) and tri-MO knockdown/ rescue assays. Hence the zebrafish assays may not be sensitive to slight losses of protein function, and/or the mutation affects a functional aspect of the protein which cannot be revealed in the zebrafish test. However, this does not exclude the presence of modifiers that are exaggerating this mild functional defect. In fact, a study by Wang et al. (2006) showed that the NTD defect and PCP defect in the cochlea can be modified by genetic background variation. They generated *Dvl1*−/−; *Dvl2*−/− double knockouts to show that although both defects were nearly 100% penetrant in an inbred 129 SvEv background,

Dvl1−/−; *Dvl2*−/− mutants showed incompletely penetrant neural tube closure defects in a mixed 129 SvEv/C57B6 background. They hypothesized that multiple dominant modifiers from the C57B6 background act together to rescue the NTD phenotype in their *Dvl1*−/−; *Dvl2*−/− mutants. While Lp^{m2Jus} is on a mixed 129:B6 background, *Lp* and Lp^{m2Jus} are on a mixed A/J:B6 and C3H:101 backgrounds respectively. Careful genotyping of *Lp* and Lp^{m2Jus} to determine the exact contribution of B6, followed by serial backcrosses to put each of the 2 mutations, $Vangl2^{S464N}$ and $Vangl2^{R259L}$, on a pure B6 background, are needed to investigate the presence of genetic modifiers of the NTD and PCP phenotypes in B6.

In addition to the looped/kinky tail phenotype, 78% of adult Lp^{m2Jus}/Lp^{m2Jus} females exhibited imperforate vagina, a phenotype previously reported for the *Lp* allele in female heterozygotes but at a much lower frequency (30-50%) (Strong and Hollander, 1949; Vandenberg and Sassoon, 2009). A recent study demonstrated an important role for *Vangl2* and non-canonical PCP signaling in establishment and maintenance cell polarity through development of the female reproductive tract (FRT) (Vandenberg and Sassoon, 2009). This remarkable increase in penetrance of the imperforate vagina in this specific Lp^{m2Jus} genetic background as compared to the *Lp* allele suggests that distinct and tissue-specific molecular mechanisms might act in parallel or interact with PCP signaling to regulate FRT development. This mutant represents an important tool to dissect such mechanisms.

Around one third of Lp^{m2Jus}/Lp^{m2Jus} males were infertile. These mice had normal mating abilities assessed by the presence of copulation plugs and did not display any abnormal reproductive tract histology or defective spermiogenesis or spermatogenesis. A reduced fertility was reported in *Fz3*+/-; *Fz6*-/- male mice; however, this was due to a marked reduction in number of sperm cells in the vas deferens suggesting that these genes may play a redundant role in sperm development and/or endocrine processes that regulate male fertility (Wang et al., 2006). In the same study, a reduced fertility in *Lp*/+ males was reported with no detailed reproductive analyses or hypothesized causes. The reduced fertility in Lp^{m2Jus}/Lp^{m2Jus} males remains unexplained and requires in depth structural and molecular studies of the reproductive system.

Compound Lp^{m2Jus}: *Lp* heterozygous embryos develop craniorachischisis and show quantitatively significant PCP inner ear defect, demonstrating that both alleles genetically interact. Interestingly, a small percentage of Lp^{m2Jus} homozygotes (12%) and Lp^{m2Jus}: *Lp* compound heterozygotes (15%) showed spina bifida. A variable phenotypic behavior for *Vangl2* was previously reported when interacting with other PCP mutants. For example, while *Vangl2: Scribble1* and *Vangl2:Dvl3* double heterozygotes develop craniorachischisis (Murdoch et al., 2001b; Etheridge et al; 2008), *Vangl2:PTK7* double heterozygotes develop spina bifida and *Vangl2: Cordon bleu* double heterozygotes develop exencephaly (Carroll et al., 2003; Lu et al., 2004). In this study, we show a variable phenotype caused by distinct mutations in the same *Vangl2* gene but in different genetic backgrounds. This variability is most likely caused by modifiers affecting the site of neural tube closure defect.

On the other hand, Lp^{m2Jus}: $Vangl1^{gt}$ double heterozygotes showed no CE or PCP defect in any of the organs studies including neural tube, eyelid and inner ear. $Vangl1^{gt}$ genetically interacts with $Vangl2^{S464N}$, with double heterozygotes developing craniorachischisis and inner ear defects (Torban et al., 2008). These data further support the importance of dosage in the Vangl signaling pathway as a modifier of the severity of the resulting phenotype. It was hypothesized that loss of 50% of *Vangl2* puts the pathway in a “sensitized” mode eliciting a phenotype from partial loss of *Vangl1* (Torban et al., 2008). However in the case of the mild Lp^{m2Jus} allele, we hypothesize that the loss of *Vangl2* activity in these double heterozygotes is not at 50% and the minimum threshold level of combined Vangl activity

required for neural tube closure is still achieved. Additional experiments are needed to test this hypothesis and to assess genetic interaction between *Lp*^{m2Jus} and *Vangl1*^{gt} when two copies of each allele are mutated for example in *Lp*^{m2Jus}/*Lp*^{m2Jus}; *Vangl1*^{gt}/+ or *Lp*^{m2Jus}/+; *Vangl1*^{gt}/*Vangl1*^{gt} mutants.

The variability in NTD phenotype incidence and severity encountered in the Vangl mouse mutants reflect to a certain extent a similar situation in human NTDs. Rare and novel missense mutations in *VANGL2* or *VANGL1* were associated with various forms of NTDs in humans, and were shown to affect the protein function *in vivo*, strongly implicating a defective PCP signaling in the pathogenesis of these malformations. When analyzed within the family, the same mutation was detected in one unaffected parent or in other moderately affected family members. It was hypothesized that mutations in these genes are of low penetrance that must interact with other undetermined genetic or environmental factors or modifiers to modulate the phenotype (Kibar et al. 2007; 2009; 2010).

We showed that the mutation R259L has no effect on gene expression and only a slight non significant effect on protein levels in brains of E16.5 homozygous embryos. We also showed that *Vangl2*^{R259L} is still present at the plasma membrane of the neuroepithelium of *Lp*^{m2Jus}/*Lp*^{m2Jus} embryos although we cannot exclude the possibility of slight alterations that were not detected in our assay. A parallel study recently published showed that the S464N and R259L variants fail to reach the plasma membrane in polarized MDCK kidney cells, and like D255E, the mutant variants are retained intracellularly in the ER, and rapidly degraded by the proteasome (Iliescu et al., 2010). In agreement with previous findings on the effect of the S464N mutation onVangl2 protein levels and membrane targeting (Torban et al., 2004; Montcouquiol et al., 2006; Devenport and Fuchs, 2008), our western blot analysis supports a similar pathogenic effect for the S464N mutation where the protein levels are reduced by one third in the brain of *Vangl2*^{S464N} (*Lp*) heterozygotes and almost completely eliminated in homozygotes. However, we did not detect any similar effect of the R259L mutation on Vangl2 protein levels by western analysis of embryonic brain tissues or on localization to plasma membrane by immunostaining of neuroepithelial cells of mutant embryos. Our results are compatible with the mild phenotype detected in the mouse *Lp*^{m2Jus} mutant and the lack of a pathogenic effect of Vangl2^{R259L} on CE in zebrafish embryos.

The dramatic effects of the Vangl2^{R259L} variant detected in the polarized MDCK kidney cells as compared to their milder effects in western and immunofluorescent studies of affected tissues could be due to the lack of *in vivo* compensatory mechanisms in cell models or to the fact that stable expression of the protein over-saturates the system with high levels of the protein that do not reflect its true physiological level. These findings stress the importance of using complementary approaches to dissect the molecular mechanisms of pathogenically- hypothesized gene variants.

ENU-induced mutagenesis represents a powerful tool for the study of gene function and generation of human disease models (Clark et al., 2004). The allelic series of mutations in the *Vangl2* gene represent an extremely valuable genetic resource for understanding this gene function in PCP signaling and for identification of genetic modifiers of the PCP and CE phenotypes in the developing neural tube, inner ear, eyelid and female reproductive tract.

MATERIALS AND METHODS

Maintenance and phenotyping of Lp^{m2Jus} mice

The *Lp*^{m2Jus} (MGI:3038827) mouse mutant with a looptail phenotype was generated and identified as part of the chromosome 4 balancer mutagenesis screens at the Mouse

Mutagenesis and Phenotyping Center for Developmental Defects in Texas Medical Center in Houston (http://www.mouse-genome.bcm.tmc.edu). The design of the chromosome 4 balancer chromosomes and the mutagenesis screens have been described elsewhere in details (Hentges et al., 2006). Briefly, mice homozygous for the chromosome 4 balancer chromosome (on a C57BL/6Brd$^{Tyr-/-}$ B6-albino genetic background), which could be visually recognized by their dark brown coat because of the presence of tyrosinase and K14-agouti transgenes at the inversion breakpoints were crossed to ENU-injected C57BL/6Brd$^{Tyr-/-}$ (albino) mice. G1 pups that were heterozygous for a potential mutation and the balancer (light brown coat) were backcrossed to balancer homozygotes (dark brown coat). G2 mice that were heterozygous for the inversion (light brown coat) were intercrossed and the offspring (G3) were analyzed. *Lp^{m2Jus}* was identified as a recessive mouse mutant with a looped tail phenotype in the G3 cross that failed to segregate to Chromosome 4. *Lp^{m2Jus}* homozygous G3 mice were outcrossed to 129S6/SvEvTac and intercrossed to regenerate the mutant phenotype at N1F1. *Lp^{m2Jus}* N1F1 mutants were archived as frozen sperm and were consequently recovered at The Jackson Laboratory (http://jaxmice.jax.org/services/) by using the Assisted In Vitro Fertilization (AIVF) method with C57BL/6J oocytes. The *Lp^{m2Jus}* mutant stock was generated and maintained by backcross and brother-sister matings. Mice were examined macroscopically for the presence of a severely “kinked” or “looped” tail. Embryos were recovered at various stages and examined for the presence of NTDs.

Two *Lp*/+ males on a mixed A/J:B6 background and four *Vangl1^{gt}/ Vangl1^{gt}* mice (2 males, 2 females) on a mixed 129:B6 background were obtained from Philippe Gros (McGill University, Montreal, Quebec). Both *Lp* and *Vangl1^{gt}* colonies were maintained by crosses to C57BL/6J mice.

DNA extraction and Genotyping

Genomic DNA was extracted from frozen liver or brain tissue using phenol-chloroform standard protocol, and from mouse tail or yolk sac using the DNeasy Blood & Tissue Kit (QIAGEN). Genotypes were confirmed for all mice included in the study. For *Lp* and *Lp^{m2Jus}* mice, genotyping was done by PCR amplification on genomic DNA for mVangl2-x3 (171 bp) and mVangl2-x7 (360bp) with these primers: mVangl2-x3F (5′-CACTATCTGGCCGTAGTTCT-3′), mVangl2-x3R (5′-CATCTGGGTCTCATCTTTGTC-3’), mVangl2-x7F (5’-GCTGTGTCACAGAGGATGAAG-3′), mVangl2-x7R (5′-ACATCCCTCCTCCGCGGCT-3′). PCR amplification was done in a total volume of 30μL containing 25-50ng genomic DNA, 80μM dNTPs, 0.25μM for each primer, 1x PCR buffer minus Mg, 1.5mM $MgCl_2$ and 1U Taq DNA polymerase (Invitrogen). PCR conditions consisted of 5 min at 94°C followed by 35 cycles with each cycle consisting of 30s at 94°C, 30s at (59°C for mVangl2-x3, 58°C for mVangl2-x7), 30s at 68°C, followed by one cycle of 5 min at 68°C. The PCR products were visualized on 1.2% agarose gel. Direct dye terminator sequencing of PCR products was done using Applied Biosystem’s 3730xl DNA Analyzer technology. The R259L mutation was also detected by AciI digestion on m*Vangl2*-exon3 PCR product and visualized on 2% agarose gel.

For *Vangl1^{gt}* mice, genotyping was done by PCR amplification on genomic DNA with 3 primers: mVangl1-exon3F (5′- AGAACAAGAGAAAGACACAAATCAC -3′), mVangl1-Intron3-R (5′- CACCAGATTTCCATGCTTGCCA -3′), GT1-R (5′-CATACTTTCGGTTCCTCTTCC CATG-3′). PCR conditions consisted of 5 min at 94°C followed by 35 cycles with each cycle consisting of 30s at 94°C, 30s at 60°C, 30s at 68°C, followed by one cycle of 5 min at 68°C. The PCR products were run on 1.2% agarose gel. Homozygous embryos showed one band at 410bp, wild-type showed one band at 744bp and heterozygous showed both bands.

Real-time PCR for mRNA quantification

Total RNA was extracted from E16.5 mouse brain with TRIzol Reagent protocol (Invitrogen). Reverse transcription were done with 1μg of total mouse brain RNA, 200 units of SuperScript II reverse transcriptase (Invitrogen), 1 mM dNTPs (Invitrogen), 300ng random primer (Invitrogen), 500ng Olido(dT)$_{12-18}$ primer and 40 units RNase Out (Invitrogen). *Vangl2* transcript levels were determined by real time PCR using the Roche Light Cycler and Taqman gene expression (ABI). We used probes specifically complementing mouse cDNA sequence of Vangl2 (Assay ID: Mm00473768_m1; Applied BioSystems). All qPCR reactions were done in triplicate for each sample with Taqman Fast qPCR Master Mix (Applied Biosystems). *Vangl2* levels were determined in fold changes, as compared with *Hprt* levels using the Roche Light Cycler software.

Western Blot analysis

E16.5 mouse brain was isolated from Lp^{m2Jus}/Lp^{m2Jus} embryos (n=7) and their wild-type littermates (n=7) and from *Lp*/+ (n=7) and *Lp/Lp* (n=6) and their wild-type littermates (n=7). Brain tissue was washed in PBS and crushed in liquid nitrogen. Protein extractions were done using RIPA buffer technique. Briefly, cold RIPA buffer (50mM Tris-HCl pH 7.4, 1% triton x-100, 0.25% Na-deochycholate, 150 mM NaCl, 1mM EDTA, 1mM phenylmethanesulfonylfluoride (PMSF), 1μg/mL of aprotinin, leupeptin and pepstatin) was added to the crushed brain and incubated at -80°C for 10 minutes. A 15 min centrifugation at 12 000 RPM was done and the surnageant, containing the protein, was recuperated. A total of 35μg of total protein was boiled in loading buffer, separated by SDS-PAGE and transferred on PVDF membrane. Membrane was blocked in 5% milk/TBS/ 0.1% tween 20 and incubated overnight at 4°C with primary antibody. Washes in TBS/0.1% tween 20 were done followed by one hour incubation at room temperature with appropriated secondary HRP-conjugate antibody (Abcam). After washes in TBP/0.1% tween 20, the membrane was incubated with SuperSignal West Pico Chemiluminescent Substrate (Thermo Scientific) and exposed on film. Western blot analysis was performed with rabbit polyclonal Vangl2 (provided by PG; 1:200) (Torban et al., 2004) and mouse monoclonal β actin (Novus Biologicals; 1:10 000) antibodies. For the Vangl2 antibody, a segment corresponding to amino acids 12-64 at the N terminus of the Vangl2 protein was used to construct a GST fusion immunogen to produce anti-Vangl2 rabbit polyclonal antisera. This antibody was demonstrated to be isoform-specific where it does not cross-react with the Vangl1 protein (Torban et al., 2004). Quantification of the protein levels was done using the program ImageJ. The Student's t-test was used to compare protein levels between wild-type and mutant embryos.

Immunofluorescence of the neural tube

E9.5 wild-type and Lp^{m2Jus}/Lp^{m2Jus} embryos (n=3 for each genotype) were isolated and fixed in 4% paraformaldehyde (PFA) at 4°C during overnight, followed by 3 washes in phosphate-buffered saline (PBS) at room temperature (RT). Overnight incubation in 30% sucrose/PBS at 4°C was done, followed by 2 hours incubation at room temperature in OCT : 30% sucrose/PBS (1:1) with gentle rocking. Tissues were then embedded in OCT and conserved at -80°C. The tissues, cut into 14μm cryosections, were fixed in 4% PFA, boiled for 6 min in 10mM citric buffer, pH 6.0 and blocked in a solution containing 10% normal inactivated goat serum/0.4% Triton in PBS for 1 hour at RT. The tissues were incubated with goat polyclonal Vangl2 (N-13) antibody (Sigma; 1:50) for 1 hour, followed by an incubation with an anti-goat alexa fluor 488 (Molecular Probes; 1:250). Sections were mounted with Prolong Gold. For negative control, PBS was used instead of the primary antibody.

Cochlear immunohistochemistry and analysis of stereociliary bundle orientation

Cochlea from E18.5 embryos were isolated under microscope and flat mounted, then fixed in 4% paraformaldehyde for 1 hour at room temperature, and washed 3X in PBS. The cochlea were then microdissected in PBS containing 0.1% triton x-100, and incubated in PBS with 5% goat serum and 0.1% triton x-100 (blocking solution) for 1 hour. This step was followed by overnight incubation with the antibody Alexa Fluor 488-conjugated phalloidin (1:40) at 4°C.Tissues were then washed 3 times in PBS with 0.1% triton x-100 at room temperature and mounted with Prolong Gold. At least 30 cells for each row at the apical region of the organ of Corti were used for quantification per sample. To determine stereociliary bundle orientation, a line was drawn through the middle of the "V"-shaped stereocilia (bisecting line). The angle formed between this line and the line parallel to the mediolateral axis was used for quantifications. In wild-type animals, this angle is close to 0 °C. Stereocilia with a deviation from normal larger than 30°C were considered to be misoriented. For statistical analysis, the Kolmogorov - Smirnov test was used to compare the distributions of the various subgroups of hair cells.

Zebrafish experiments

The open reading frame (ORF) of *VANGL2* (Accesssion nb: NM_020335) was amplified from total human RNA by RT-PCR and the resulting fragment was cloned into pCS2+ using ClaI and XhoI sites built in the PCR primers. The R259L variant introduced in the human *VANGL2* ORF cloned into pCS2+. The mutagenic primer used was: 5′-GACGGCGCCAGCC**T**CTTCTACAACGTTG-3′. All constructs were verified by sequencing. Sense capped RNA was synthesized using the mMESSAGE mMACHINE transcription kit (Ambion) as described by the manufacturer.

Longfin zebrafish were raised from a colony maintained according to established procedures in compliance with guidelines set out by the Canadian Council for Animal Care. Injections were performed in oocytes at the one to four cell stage. The vital dye fast-green was incorporated to the injection vehicle to monitor injection quality (0.1%; Sigma). For the overexpression assay, 50 or 100 or 200pg of human *VANGL2* RNA was used. Body length was assessed at 2 days post fertilization. To knockdown translation of the zebrafish *tri/VANGL2*, ~7 ng of the previously described *tri*-MO antisense morpholino oligonucleotide was injected. To rescue the phenotype, 50 pg of human *VANGL2* RNA was co-injected with the *tri*-MO.

For statistical analyses, since the measurements of zebrafish body length were not normally distributed, the Kruskal-Wallis test was used to compare differences between experimental groups, followed by Dunn's comparison as a post-hoc test (GraphPad Prism). We considered groups statistically significantly different from the control group if the *P* value was less than 0.05. Cluster analysis was done using the SSPS statistics software. A Chi-square test was used to analyze the difference in distribution of the clusters among the experimental groups.

Supplementary Material

Refer to Web version on PubMed Central for supplementary material.

Acknowledgments

We would like to thank Farida Kibar for her help in statistical analyses, Stephanie Lachance and Cynthia Horth for their technical assistance and Edna Brustein for the technical support on zebrafish experiments.

Grant Sponsor: the Canadian Institutes for Health Research; Grants number: 86520 (Z.K.) and MT-13425 (P.G.). Grant Sponsor: the Natural Science and Engineering Research Council, Genome Quebec and Genome Canada (P.D.). Grant Sponsor: the National Institutes of Health; Grants number: U01 HD39372 and R01 CA115503 (M.J.).

References

Bassuk AG, Kibar A. Genetic basis of neural tube defects. Semin Pediatr Neurol. 2009; 16:101–110. [PubMed: 19778707]

Carroll EA, Gerrelli D, Gasca S, Berg E, Beier DR, Copp AJ, Klingensmith J. *Cordon-bleu* is a conserved gene involved in neural tube formation. Dev Biol. 2003; 262:16–31. [PubMed: 14512015]

Devenport D, Fuchs E. Planar polarization in embryonic epidermis orchestrates global asymmetric morphogenesis of hair follicles. Nat Cell Biol. 2008; 10:1257–1268. [PubMed: 18849982]

Etheridge SL, Ray S, Li S, Hamblet NS, Lijam N, Tsang M, Greer J, Kardos N, Wang J, Sussman DJ, Chen P, Wynshaw-Boris A. Murine dishevelled 3 functions in redundant pathways with dishevelled 1 and 2 in normal cardiac outflow tract, cochlea, and neural tube development. PLoS Genet. 2008; 4:e1000259. [PubMed: 19008950]

Clark AT, Goldowitz D, Takahashi JS, Vitaterna MH, Siepka SM, Peters LL, Frankel WN, Carlson GA, Rossant J, Nadeau JH, Justice MJ. Implementing large-scale ENU mutagenesis screens in North America. Genetica. 2004; 122:51–64. [PubMed: 15619961]

Gravel M, Iliescu A, Horth C, Apuzzo S, Gros P. Molecular and cellular mechanisms underlying neural tube defects in the loop-tail mutant mouse. Biochemistry. 2010; 49:3445–3455. [PubMed: 20329788]

Henderson DJ, Conway SJ, Greene ND, Gerrelli D, Murdoch JN, Anderson RH, Copp AJ. Cardiovascular defects associated with abnormalities in midline development in the Loop-tail mouse mutant. Circ Res. 2001; 89:6–12. [PubMed: 11440971]

Hentges KE, Nakamura H, Furuta Y, Yu Y, Thompson DM, O'Brien W, Bradley A, Justice MJ. Novel lethal mouse mutants produced in balancer chromosome screens. Gene Expr Patterns. 2006; 6:653–665. [PubMed: 16466971]

Iliescu A, Gravel M, Horth C, Kibar Z, Gros P. Loss of membrane targeting of vangl proteins causes neural tube defects. Biochemistry. 2010 Epub ahead of print.

Jessen JR, Topczewski J, Bingham S, Sepich DS, Marlow F, Chandrasekhar A, Solnica-Krezel L. Zebrafish *trilobite* identifies new roles for *Strabismus* in gastrulation and neuronal movements. Nat Cell Biol. 2002; 4:610–615. [PubMed: 12105418]

Keller R, Shook D, Skoglund P. The forces that shape embryos: physical aspects of convergent extension by cell intercalation. Phys Biol. 2008; 5:015007. [PubMed: 18403829]

Kibar Z, Underhill DA, Canonne-Hergaux F, Gauthier S, Justice MJ, Gros P. Identification of a new chemically induced allele (Lp^{m1Jus}) at the loop-tail locus: morphology, histology, and genetic mapping. Genomics. 2001a; 72:331–337. [PubMed: 11401449]

Kibar Z, Vogan KJ, Groulx N, Justice MJ, Underhill DA, Gros P. *Ltap*, a mammalian homolog of Drosophila *Strabismus/Van Gogh*, is altered in the mouse neural tube mutant Loop-tail. Nat Genet. 2001b; 28:251–255. [PubMed: 11431695]

Kibar Z, Torban E, McDearmid JR, Reynolds A, Berghout J, Mathieu M, Kirillova I, De Marco P, Merello E, Hayes JM, Wallingford JB, Drapeau P, Capra V, Gros P. Mutations in *VANGL1* are associated with neural tube defects in humans. New Engl J Med. 2007; 35:1432–1437. [PubMed: 17409324]

Kibar Z, Bosoi CM, Kooistra M, Salem S, Finnell RH, De Marco P, Merello E, Bassuk AG, Capra V, Gros P. Novel mutations in *VANGL1* in neural tube defects. Hum Mutat. 2009; 30:E706–715. [PubMed: 19319979]

Kibar Z, Salem S, Bosoi CM, Pauwels E, De Marco P, Merello E, Bassuk AG, Capra V, Gros P. Contribution of *VANGL2* mutations to isolated neural tube defects. Clin Genet. 2010

Lei YP, Zhang T, Li H, Wu BL, Jin L, Wang HY. *VANGL2* mutations in human cranial neural-tube defects. N Engl J Med. 2010; 62:2232–2235. [PubMed: 20558380]

Lu X, Borchers AG, Jolicoeur C, Rayburn H, Baker JC, Tessier-Lavigne M. *PTK7/CCK-4* is a novel regulator of planar cell polarity in vertebrates. Nature. 2004; 430:93–98. [PubMed: 15229603]

McNeill H. Planar cell polarity: keeping hairs straight is not so simple. Cold Spring Harb Perspect Biol. 2010; 2:a003376. [PubMed: 20182624]

Merte J, Jensen D, Wright K, Sarsfield S, Wang Y, Schekman R, Ginty DD. Sec24b selectively sorts Vangl2 to regulate planar cell polarity during neural tube closure. Nat Cell Biol. 2010; 12:41–46. [PubMed: 19966784]

Montcouquiol M, Rachel RA, Lanford PJ, Copeland NG, Jenkins NA, Kelley MW. Identification of *Vangl2* and *Scrb1* as planar polarity genes in mammals. Nature. 2003; 423:173–177. [PubMed: 12724779]

Montcouquiol M, Sans N, Huss D, Kach J, Dickman JD, Forge A, Rachel RA, Copeland NG, Jenkins NA, Bogani D, Murdoch J, Warchol ME, Wenthold RJ, Kelley MW. Asymmetric localization of Vangl2 and Fz3 indicate novel mechanisms for planar cell polarity in mammals. J Neurosci. 2006; 26:5265–5275. [PubMed: 16687519]

Murdoch JN, Doudney K, Paternotte C, Copp AJ, Stanier P. Severe neural tube defects in the loop-tail mouse result from mutation of *Lpp1*, a novel gene involved in floor plate specification. Hum Mol Genet. 2001a; 10:2593–2601. [PubMed: 11709546]

Murdoch JN, Rachel RA, Shah S, Beermann F, Stanier P, Mason CA, Copp AJ. *Circletail*, a new mouse mutant with severe neural tube defects: chromosomal localization and interaction with the *loop-tail* mutation. Genomics. 2001b; 78:55–63. [PubMed: 11707073]

Park M, Moon RT. The planar cell-polarity gene *Stbm* regulates cell behavior and cell fate in vertebrate embryos. Nat Cell Biol. 2002; 4:20–25. [PubMed: 11780127]

Reynolds A, McDearmid JR, Lachance S, De Marco P, Merello E, Capra V, Gros P, Drapeau P, Kibar Z. *VANGL1* rare variants associated with neural tube defects affect convergent extension in zebrafish. Mech Dev. 2010; 127:385–392. [PubMed: 20043994]

Simons M, Mlodzik M. Planar cell polarity signaling: from fly development to human disease. Annu Rev Genet. 2008; 42:517–540. [PubMed: 18710302]

Strong LC, Hollander WF. Hereditary Loop-tail in the house mouse. J Hered. 1949; 40:329–334.

Suriben R, Kivimäe S, Fisher DA, Moon RT, Cheyette BN. Posterior malformations in *Dact1* mutant mice arise through misregulated *Vangl2* at the primitive streak. Nat Genet. 2009; 41:977–985. [PubMed: 19701191]

Torban E, Wang H-J, Groulx N, Gros P. Independent mutations in mouse *Vangl2* that cause neural tube defects in looptail mice impair interaction with members of the Dishevelled family. J Biol Chem. 2004; 279:52703–52713. [PubMed: 15456783]

Torban E, Patenaude AM, Leclerc S, Rakowiecki S, Gauthier S, Andelfinger G, Epstein DJ, Gros P. Genetic interaction between members of the *Vangl* family causes neural tube defects in mice. Proc Natl Acad Sci U S A. 2008; 105:3449–3454. [PubMed: 18296642]

Vandenberg AL, Sassoon DA. Non-canonical Wnt signaling regulates cell polarity in female reproductive tract development via van gogh-like 2. Development. 2009; 136:1559–1570. [PubMed: 19363157]

Vladar EK, Antic D, Axelrod JD. Planar Cell Polarity Signaling: The Developing Cell's Compass. Cold Spring Harb Perspect Biol. 2009; 1:a002964. [PubMed: 20066108]

Wallingford JB. Neural tube closure and neural tube defects: studies in animal models reveal known knowns and known unknowns. Am J Med Genet C Semin Med Genet. 2005; 135:59–68. [PubMed: 15806594]

Wang J, Hamblet NS, Mark S, Dickinson ME, Brinkman BC, Segil N, Fraser SE, Chen P, Wallingford JB, Wynshaw-Boris A. Dishevelled genes mediate a conserved mammalian PCP pathway to regulate convergent extension during neurulation. Development. 2006; 133:1767–1778. [PubMed: 16571627]

Wang Y, Guo N, Nathans J. The role of Frizzled3 and Frizzled6 in neural tube closure and in the planar polarity of inner-ear sensory hair cells. J Neurosci. 2006; 26:2147–2156. [PubMed: 16495441]

Wang Y, Nathans J. Tissue/planar cell polarity in vertebrates: new insights and new questions. Development. 2007; 134:647–658. [PubMed: 17259302]

Ybot-Gonzalez P, Savery D, Gerrelli D, Signore M, Mitchell CE, Faux CH, Greene ND, Copp AJ. Convergent extension, planar-cell-polarity signalling and initiation of mouse neural tube closure. Development. 2007; 134:789–799. [PubMed: 17229766]

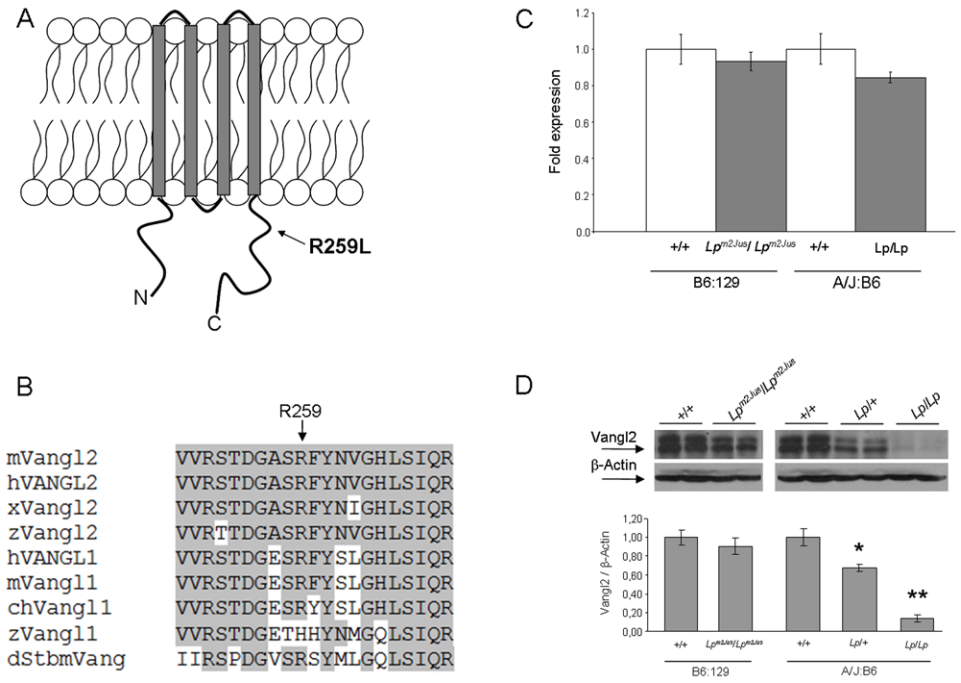

Figure 1.

Molecular characterization of the *Lp^m2Jus* mutant. Panel A. Diagram of the Vangl2 protein structure with the approximate position of the R259L mutation identified in *Lp^m2Jus* indicated by an arrow. Panel B. Partial alignment of mouse Vangl2 with 8 other Vangl/Stbm sequences. Residues conserved between Vangl2 and other family members are highlighted. The R259L variant affects a highly conserved amino acid residue (indicated by an arrow). Accession numbers: mouse Vangl2 (mVangl2), NP_277044; human VANGL2 (hVANGL2), NP_065068; frog Vangl2 (xVangl2), AAK70879; zebrafishVangl2 (zVangl2), NP_705960; human VANGL1 (hVANGL1), NP_620409; mouse Vangl1 (mVangl1), NP_808213; chicken Vangl1 (chVangl1), XP_001232441; zebrafishVangl1 (zVangl1), AAQ84560; and Drosophila Stbm (dStbm), NP_477177. Panel C. Real- time PCR showing the relative levels of *Vangl2* mRNA compared with *Hprt* transcripts in brain tissues of E16.5 wild-type and mutant embryos. Panel D. Western analysis of Vangl2 protein levels in brain tissues of E16.5 wild-type and mutant embryos. β-actin was used as an internal control. Top, western blots of two representative embryos per group are shown. Bottom, a histogram showing the relative levels of Vangl2 protein compared with β-actin. A significant difference was detected between wild-type and *Lp*/+ (**P*<0.001) and between wild-type and *Lp/Lp* embryos (***P*<0.0001).

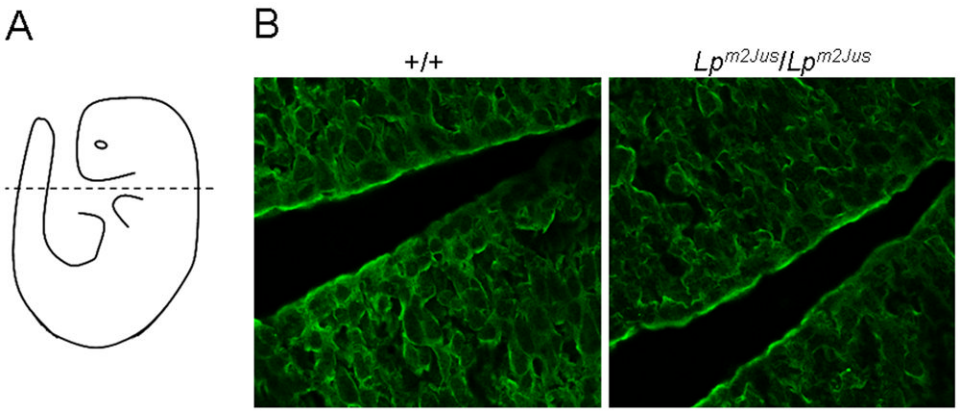

Figure 2.
Localization of the Vangl2 protein in neural tube of wild-type and Lp^{m2Jus}/Lp^{m2Jus} embryos. (A) A diagrammatic representation of a mouse embryo indicating the level and plane of section. (B) Vangl2 protein is present and membrane-associated in the neural tube of wild-type (+/+) and of homozygous (Lp^{m2Jus}/Lp^{m2Jus}) mouse embryos. 630x magnification.

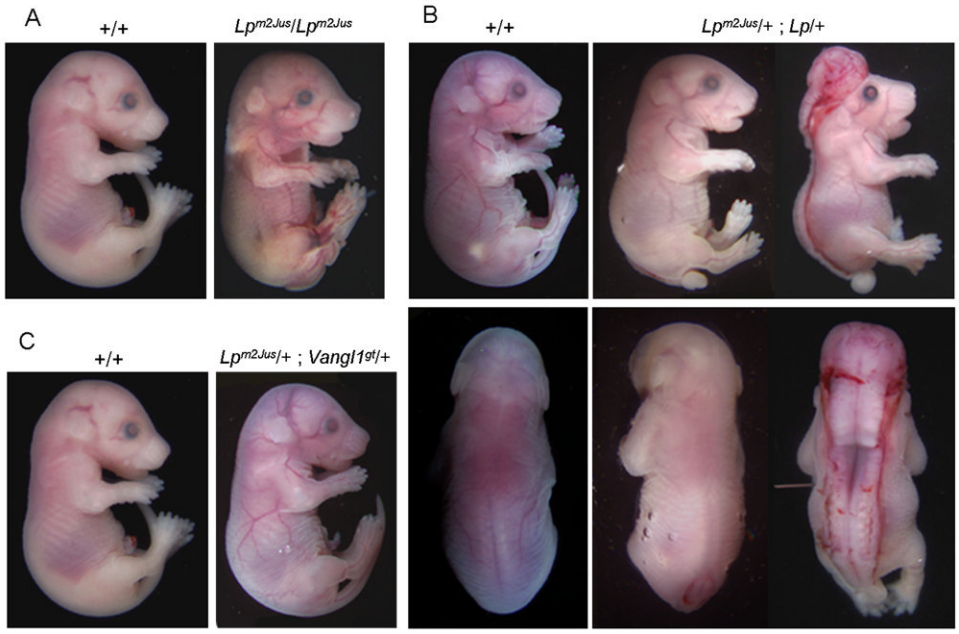

Figure 3.
Morphological appearance of *Lp*^{m2Jus} homozygotes (panel A), *Lp*^{m2Jus}*/Lp* (panel B) double heterozygotes and *Lp*^{m2Jus}*/Vangl1*^{gt} (panel C) at E18.5.

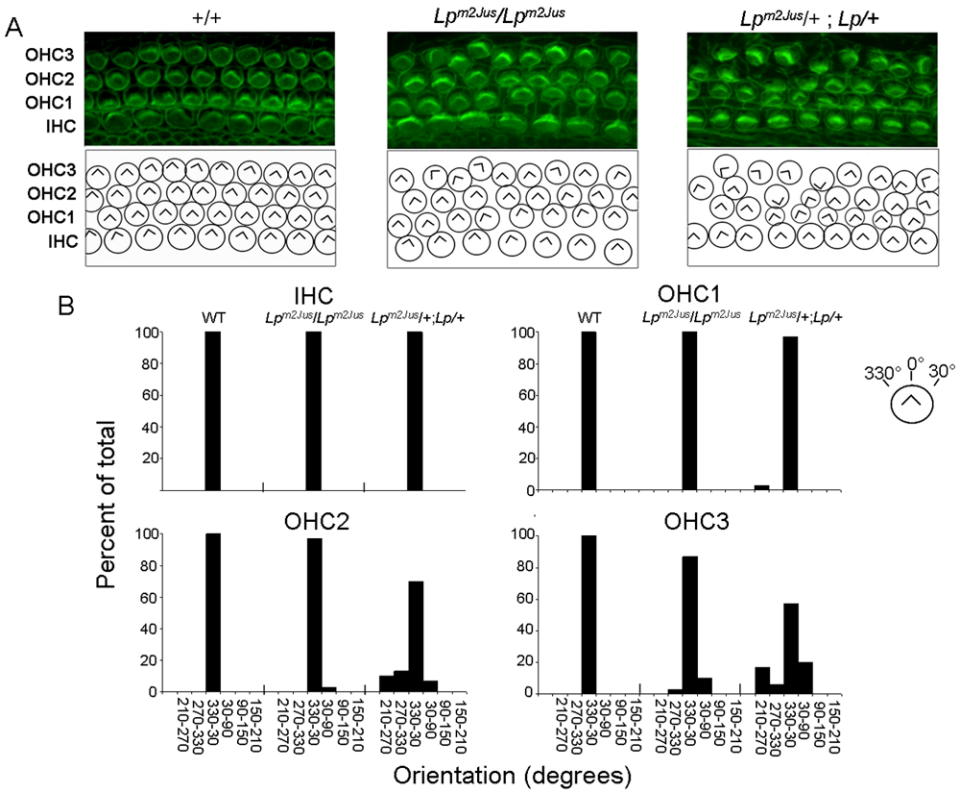

Figure 4.

Comparison of hair bundle orientation defects at the apical region of the organ of Corti in WT, *Lp*^{m2Jus}/ *Lp*^{m2Jus} and *Lp*^{m2Jus}/+; *Lp*/+ at E18.5. Panel A, Top, Stereocilia labeled with phalloidin (green). Bottom, Diagrams showing the scoring of hair bundle orientation for the images above. IHC, Inner hair cells; OHC1, Inner row of outer hair cells; OHC2, central row of outer hair cells; OHC3, outer row of outer hair cells. The genotype is indicated above each column of panels. Panel B. Quantification of the IHC, OHC1, OHC2, and OHC3 bundle orientations for each of the three genotypes indicated above based on phalloidin staining. The convention for angular measurements is shown in the top right corner of the panel. Statistical analysis was done by the Kolmogorov - Smirnov test (P=0.005 for OHC2 and OHC3 of the *Lp*^{m2Jus}/+; *Lp*/+ as compared to the wild-type).

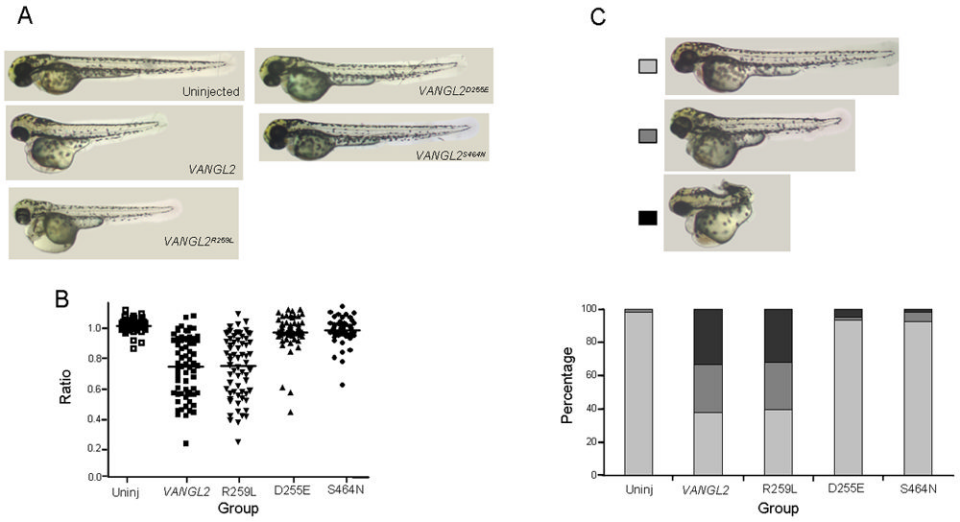

Figure 5.

Effect of overexpression of *VANGL2*^{R259L} variant on convergent extension in zebrafish embryos. Panel A, lateral views of 2 days post fertilization zebrafish including uninjected wild-type and fish injected with 200 pg of either *VANGL2* or *VANGL2*^{R259L} or *VANGL2*^{D255E} or *VANGL2*^{S464N}. Panel B, statistical analyses of the body length measurements of all 5 groups indicated above. The Kruskal-Wallis test was used to compare differences between experimental groups (P<0.001 for *VANGL2* and *VANGL2*^{R259L} as compared to the uninjected fish and P<0.001 for *VANGL2*^{D255E} or *VANGL2*^{S464N} as compared to *VANGL2*). Panel C, Top, lateral views of 2 days post fertilization zebrafish from the 3 clusters identified based on phenotype severity. Bottom, the distribution of the 3 clusters in each of the 5 experimental groups (χ^2 test, P<0.05 for *VANGL2* and *VANGL2*^{R259L} as compared to the uninjected fish and P<0.05 for *VANGL2*^{D255E} or *VANGL2*^{S464N} as compared to *VANGL2*).

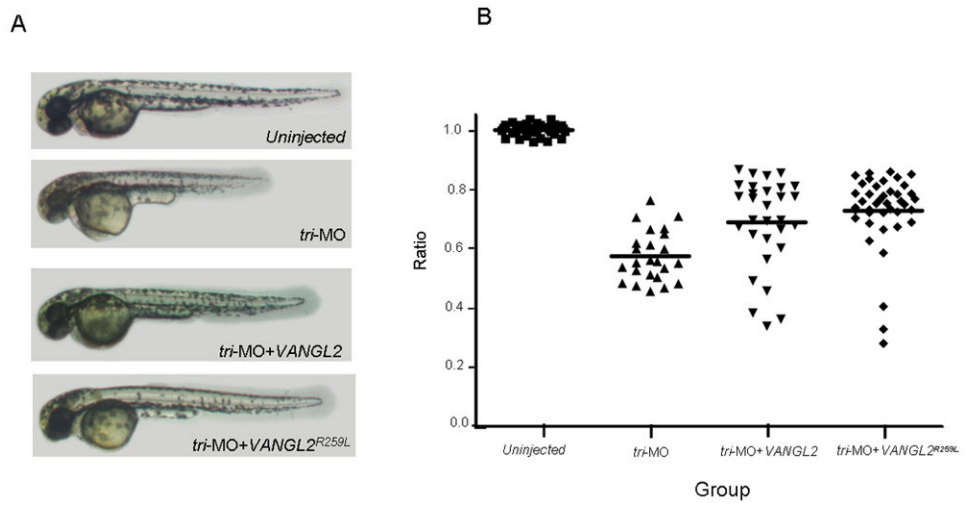

Figure 6.

Ability of *VANGL2*^{R259L} variant to rescue the convergent extension defect in zebrafish embryos treated with tri-MO. Panel A, lateral views of 2 days post fertilization zebrafish including uninjected wild-type and fish injected with either *tri*-MO alone, or *tri*-MO + *VANGL2* or *tri*-MO+ *VANGL2*^{R259L}. Panel B, statistical analyses of the body length measurements of all 4 groups indicated above. The Kruskal-Wallis test was used to compare differences between experimental groups (P<0.001 for *tri*-MO vs uninjected; P<0.05 and P<0.01 for *VANGL2* and *VANGL2*^{R259L} as compared to the *tri*-MO alone respectively).

Table 1

Genotype-phenotype studies of the *Lp*^{m2Jus} looptail mutant

R259L genotype at the *Vangl2* locus		**Phenotype**			
		Looped or kinky tail	**Spina bifida**	**Imperforate vagina**	**Male infertility**
Adult (n=241)	36 +/+, 141 +/- (99 ♀, 78 ♂)	0	NA	0	0[b]
	64 -/- (27 ♀, 37 ♂)	30 (47%)	NA	21 (78%)	12 (32%)
E16.5-E18.5 (n=156)	37 +/+, 69 +/-	0	0	NA	NA
	50 -/-	16 (32%) [a]	6 (12%)	NA	NA

[a] This frequency could be underestimated due to the difficulty in visual examination of the looped or kinky tail in embryos.

[b] Absence of male infertility is confirmed only in 4 +/+ and 29 +/- males included in the breeding scheme.